October 2023

Labile Dissolved Nickel (Ni) Concentrations in the North Pacific

Calyn M. Crawford
University of South Florida

Labile Dissolved Nickel (Ni) Concentrations in the North Pacific

by

Calyn M. Crawford

A thesis submitted in partial fulfillment
of the requirements for the degree of
Master of Science
College of Marine Science
University of South Florida

Co-Major Professor: Kristen N. Buck, Ph.D.
Co-Major Professor: Brad Rosenheim, Ph.D.
Mya Breitbart, Ph.D.

Date of Approval:
October 20, 2023

Keywords: trace metals, biogeochemistry, organic ligands, bioavailability

Dedication

Be not afraid of growing slowly; be afraid only of standing still.

-Chinese Proverb

Dedicated to all the family, friends, colleagues, and mentors who have helped me grow.

Table of Contents

List of Tables

List of Figures

Abstract

Nickel (Ni) is an important micronutrient for phytoplankton and bacteria that serves as a required co-factor in several metalloenzymes. Despite these known biological uses, total dissolved Ni concentrations remain elevated in global surface waters, in contrast to the surface depletion commonly observed for macronutrients and other nutrient-type trace elements. A prevailing hypothesis for the muted depletion of dissolved Ni concentrations in surface waters is that dissolved Ni in seawater is not in a bioavailable form. The chemical lability of Ni in seawater provides insight into Ni speciation and bioavailability, but few measurements have been made in the open ocean to date. Here we present the first depth profiles of measured labile Ni concentrations in the upper ocean water column (to 1,000 m). Measurements were performed at eight stations across three distinct biogeochemical regimes in the Northeast Pacific Ocean, namely coastal upwelling in the Northeast Pacific, the subtropical gyre, and iron-limited waters of the subarctic Pacific at Ocean Station Papa. Labile Ni concentrations were generally nutrient-type in the profiles, with lowest concentrations associated with fluorescence maxima, including near complete depletion in the subsurface fluorescence maximum of the oligotrophic gyre, and increasing labile Ni observed with macronutrient regeneration and silica frustule dissolution at depth. Deviations from a classic nutrient-type profile were evident in a surface maximum of labile dissolved Ni and an apparent deficit in the deepest samples, which may reflect distinct sources and sinks of this chemical form of dissolved Ni. Samples in this study were accidentally buffered to pH 9.0 instead of the calibration pH of 8.4, which may have resulted in an

overestimation of labile Ni throughout the dataset, necessitating further research into the sensitivity of this operationally-defined method to pH changes.

Chapter One: Labile Dissolved Nickel (Ni) Concentrations in the North Pacific

Note to Reader:

This chapter was produced as part of a collaborative study aboard the *R/V Sikuliaq* during the 2022 Iron (Fe) Ocean Acidification Cruise (FeOA). I contributed to sample collection at sea and conducted the labile dissolved Ni concentration analyses for this chapter. Fellow members of the Buck laboratory helped with the deployment and recovery of sampling systems to collect my project samples. Hydrographic data from the Buck laboratory trace metal clean rosette system were processed by Dr. Salvatore Caprara, and Caitlyn Parente measured the concentrations of macronutrients in discrete samples.

Introduction

Many trace metals in the world's oceans serve as important micronutrients for use in biological processes as key components of metalloenzymes (Sunda 1989). As such, the bioavailability of trace metals can influence primary production (Martin 1990), phytoplankton community composition (Moore et al. 2001) and macronutrient acquisition and cycling (Moore et al. 2013). Therefore, a more concrete understanding of the bioavailability and cycling of these critical elements warrants further investigation if we wish to understand oceanic ecosystems more completely.

The trace metal nickel (Ni) is an essential co-factor in enzymes used by phytoplankton for cell protection (Qiu and Price 2009), dissolved organic nitrogen (DON) acquisition (Price and Morel 1991), and by marine heterotrophs for glucose transformation (Mazzotta et al. 2021).

Superoxide dismutase (SOD) enzymes catalyze the redox reaction of superoxide, a toxic free radical species produced as a byproduct of photosynthesis, to oxygen and hydrogen peroxide (Fridovich 1997). The Ni-containing SOD isoform is widely used by marine phytoplankton, and is the only SOD in cyanobacteria, which as a result have an obligate Ni requirement for growth (Dupont et al. 2008). In oligotrophic environments, where inorganic nutrient concentrations are exceedingly low, phytoplankton often meet their nitrogen requirement by taking up urea, a form of DON whose acquisition is reliant on use of the Ni-containing urease enzyme (Antia et al. 1975). This reliance can lead to nickel-nitrogen (Ni-N) colimitation for phytoplankton growing on urea as their sole source of nitrogen (Price and Morel 1991; Dupont et al. 2010). Most recently, a widespread marine heterotroph, *Pseudoalteromonas*, was also found to use Ni when transitioning between glucose and fructose sugar sources (Mazzotta et al. 2021). The use of Ni in glucose metabolism by heterotrophic bacteria is the first documented example of Ni acquisition by heterotrophs and highlights potential demand for Ni outside the euphotic zone.

Dissolved (<0.2 μm filtered) Ni (dNi) exhibits a nutrient-like profile in the ocean (Sclater et al. 1976; Bruland 1980; Bruland and Franks 1983) with low surface concentrations reflecting biological uptake and increasing concentrations at depth below the euphotic zone as Ni is remineralized from sinking biological material. Notably, Ni appears to have a dual regeneration process, with dNi concentrations increasing initially with phosphate and nitrate at shallower depths (<800 m) and then again with silicic acid in deeper (>800 m) waters. This has been attributed to a shallower regeneration cycle of Ni from organic matter and a deeper one from Ni release during diatom frustule dissolution (Bruland 1980). Synchrotron analyses of Ni distributions within diatom cells have shown Ni in both the internal organic matter of cells and in

the frustules, with frustules contributing 50% of diatom cellular Ni concentrations (Twining et al. 2011).

As with other nutrient-type elements, dissolved Ni concentrations are higher in the older, deep waters of the North Pacific (Bruland 1980) relative to the North Atlantic (Sclater et al. 1976). However, unlike other nutrient-type metals, surface concentrations of dNi remain relatively high (typically above 2 nM), even in the open ocean (Sclater et al. 1976; Bruland 1980; Boyle et al. 1981). This is surprising since Ni demand is presumably highest in open ocean surface waters, due to the obligate Ni requirement for NiSOD in cyanobacteria (Dupont et al. 2008), regulation of nitrogen fixation rates by diazotrophs (Ho 2013), and the importance of Ni for urease (Price and Morel 1991) to acquire organic nitrogen in surface waters with limited nitrate. This apparent lack of drawdown of dNi in oligotrophic surface waters has been hypothesized to reflect that the dNi pool is not sufficiently bioavailable to phytoplankton (Mackey et al. 2002).

The bioavailability of trace metals is governed by the speciation, or different chemical forms, of dissolved metals in seawater. The total concentration of dissolved metal (M_T) in a sample is defined as the sum of dissolved organic (ML) and inorganic (M') metal species (Eq. 1). At the cellular level, trace metals are taken up by phytoplankton when free, hydrated metal ions (M^{n+}) bind to transport sites on the cell membrane (Sunda 1989). The bioavailability of trace metals for phytoplankton is described in the Free Ion Model and is a function of the concentration of M^{n+}, included in M' (Sunda 1989).

$$Eq\ 1. \quad M_! = [ML] + [M^{"}]$$

The concentration of M^{n+} in solution is reduced by complexation with organic ligands (L), which converts more of the M_T to ML (Sunda 1989). The removal of the most bioavailable form M^{n+} and subsequent conversion to organic complexes reduces the bioavailability of metals to phytoplankton and decouples dissolved metal concentrations ($[M_T]$) from bioavailability.

Measuring the bioavailability of trace metals in seawater is challenging, as it requires distinguishing between inorganic and organic forms of elements that are present in seawater at very low (nM) concentrations. There are two main approaches based on the electrochemical method competitive ligand exchange adsorptive cathodic stripping voltammetry (CLE-AdCSV). In forward titrations with CLE, natural ligands in the sample are titrated with metal additions and a competitive (added) ligand equilibrates with the target metal and natural ligands in a sample to form a metal-added ligand complex (ML_{add}). The concentration of the resulting ML_{add} complex is measured by AdCSV, whereby ML_{add} is adsorbed onto a hanging mercury drop electrode (HMDE) and quantified by cathodic stripping voltammetry. This method measures the concentrations and conditional stability constants of metal binding organic ligands present in the sample. Along with dissolved metal concentrations, these measurements can be used to calculate M' and M^{n+} from equilibrium equations. However, this method best characterizes the ligands titrated in the sample and is thus limited to those with ligand (L) concentrations present in excess of total dissolved metal (M_T) concentrations (Gledhill and Buck 2012).

The first application of this method to Ni found that a sizable portion (~40%) of Ni was not organically complexed (Van den Berg and Nimmo 1987) and dissolved Ni concentrations exceeded Ni-binding ligand concentrations. This leads to more M compared to L in surface waters, precluding the use of CLE-AdCSV with forward titrations. More recent studies of Ni bioavailability and speciation have focused on measuring the concentration of "labile" dissolved

Ni by using a competitive added ligand to bind any Ni in the sample that is not organically complexed or will otherwise exchange with the added ligand, and then measuring the resulting ML_{add} by standard addition (Saito et al. 2004; Boiteau et al. 2016). When Ni concentrations are higher than natural Ni-binding ligand concentrations, this approach allows an operationally defined measurement of labile Ni that is meant to approximate Ni' in the samples.

Early work focused on estuarine environments found that anthropogenic ligands such as ethylenediaminetetraacetic acid (EDTA) complex dNi in the environment (Van den Berg and Nimmo 1987) and may be especially important for speciation in coastal systems (Bedsworth and Sedlak 1999). However, only two studies have measured labile Ni in open ocean waters, both focused on surface waters (Saito et al. 2004; Boiteau et al. 2016). On a transect through the Peru upwelling region, ~50-100% of total dissolved Ni (dNi) was found to be labile Ni species (Saito et al. 2004). Similar results were reported in surface waters from a zonal transect off Peru, where the majority of dNi (48-78%) was labile (Boiteau et al. 2016). Recent culture studies have also shown that Ni in oligotrophic surface seawater can be rapidly depleted by phytoplankton when supplemented with ample macronutrients (John et al. 2022). These datasets altogether suggest that dNi in the surface ocean is largely labile and bioavailable. Thus, it remains difficult to reconcile the paradox of dNi profiles in the global ocean.

In this study, labile dissolved Ni concentrations were measured using CLE-AdCSV in eight depth profiles collected from the upper 1,000 m of the water column in the Northeast Pacific. The stations encompassed three distinct biogeochemical regimes: coastal upwelling, oligotrophic gyre, and high nutrient low chlorophyll (HNLC) waters. These data constitute the first depth profiles of Ni speciation in the oceans to date, allowing a first look at how bioavailable Ni concentrations vary with depth across these regimes.

Methods

Sample collection

Depth profiles to ~1,000 m were sampled at eight stations in the North Pacific aboard the *R/V Sikuliaq* in June 2022 using a trace metal clean rosette system (Seabird) outfitted with trace metal clean modified 12-L x-Niskin samplers (OceanTestEquipment, Inc.) and deployed on ¼" Amsteel synthetic line. Surface samples were collected using a trace metal clean "towfish" sampler deployed at ~2 m depth (Mellett and Buck 2020) on approach to each station (Fig. 1). Fluorinated high-density polyethylene sample bottles (500 mL, Nalgene) were cleaned prior to collection of Ni speciation samples following the GEOTRACES cookbook (Cutter et al. 2017), and triple rinsed with filtered (<0.2 μm, Pall Acropak) seawater sample prior to filling. Filtered samples were then stored in a refrigerator at 4 °C until analyzed shipboard, typically within seven days. Remaining samples were frozen at -20 °C and transported to the University of South Florida (USF) for shore-based analyses. Total dissolved Ni samples were filtered using a 0.2 μm filter (SUPOR AcroPak) into 125 mL LDPE bottles (Nalgene) that were triple rinsed with filtered seawater. These were then acidified to pH <1.8 using 0.024 M QHCl and stored at room temperature until analyzed by mass spectrometry at USF.

Labile dissolved Ni concentrations

Labile dissolved Ni concentrations were determined by equilibration of buffered seawater samples with the added ligand dimethylglyoxime (DMG). Briefly, 10-mL sample aliquots were partitioned into Teflon vials (Savillex) that had been acid-cleaned and preconditioned with Milli-Q, borate buffer, and DMG. Samples were originally intended to be buffered with 7.5 mM borate in 0.4 N Q-NH_4OH buffer to maintain a sample pH of ~8.1 but were accidentally spiked with 50 mM borate in 0.8 N Q-NH_4OH resulting in a pH of ~9.0. All measurements were made at the

same pH with the same reagents so although the results have not been assessed as a function of these pH differences, they can be compared within this study across the different biogeochemical regimes sampled. The added ligand DMG was added to a final concentration of 200 µM (Boiteau et al. 2016) and after an overnight (>12 h) equilibration, samples were analyzed on a BioAnalytical Systems (BASi) controlled-growth mercury electrode (drop size 10) connected to an Epsilon 2 analyzer (Dupont et al. 2010). Samples were purged for 120 s with high purity nitrogen gas while stirring (Saito et al. 2004), and then analyzed in triplicate for labile Ni. Labile Ni concentrations were determined by standard additions (1 nM) of dissolved Ni made in the same electrochemical cell as the initial sample measurements. All measurements were conducted in triplicate using a 15 s deposition time and linear sweep from -0.7 to -1.4 V at a rate of 10 V s^{-1}. Raw data were processed using ECDSoft to measure peak heights (Omanović et al. 2015) and labile Ni concentrations determined from the initial replicate sample measurements and the slope of the Ni additions.

Dissolved macronutrient concentrations

Samples for dissolved macronutrient analysis were filtered through 0.2 µm (Pall Acropak) filters following the same approach as the labile dissolved Ni concentration samples and collected in acid-cleaned 15 mL polypropylene tubes (Falcon, Fisher Scientific). These filtered samples were maintained at 4˚C via refrigeration until analysis at sea on a QuAAtro39 AutoAnalyzer (Seal Analytical) within 24 hours of collection. A 9-point calibration curve of macronutrient standards was prepared daily from stock solutions and the concentrations of nitrate+nitrite (N+N, "nitrate"), nitrite, soluble reactive phosphorus ("phosphate") and silicic acid in the samples were determined based on this curve. Chemical reagents were remade every 2 weeks or if contamination was suspected (Strickland and Parsons 1972; Parsons et al. 1984;

Gordon et al. 1993), and limits of detection for each parameter were determined from three times the standard deviation of the lowest detectable standard for each parameter.

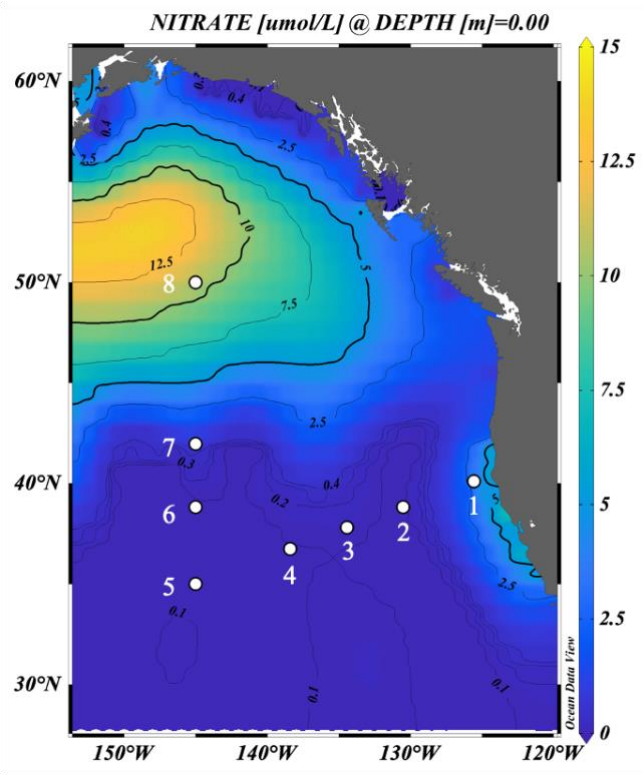

Figure 1. Map showing locations of eight stations sampled for depth profiles of the upper 1,000 m in the Northeast Pacific Ocean overlaid on average nitrate data in the month of June from the World Ocean Atlas 2018. Samples were collected using trace metal clean techniques aboard the *R/V Sikuliaq* as part of the iron bioavailability ocean acidification (FeOA) cruise in June 2022.

Results

Overall, the upper 250 m of profiles held the most variance in temperature and salinity (Fig. 2A, 3A, 4A, S2). Mixed layer depths were between 5 and 40 m, with the deepest mixed layers in the subtropical gyre (Fig. 3A, Table 1). Labile dissolved Ni concentrations were generally lower in the upper water column and increased with depth (Fig. 2C, 3C, 4C, S3), although subsurface minima in labile Ni were common in the euphotic zone and were often associated with the subsurface fluorescence maxima (Fig. 3C, 4C). In surface waters, labile Ni concentrations ranged from 1.6 ± 0.3 to 4.5 ± 0.4 nM (Fig. 2C, 3C, 4C, S4). The lowest

concentration of labile Ni in this dataset, 0.49 ± 0.08 nM, was at 90 m depth in Station 5, just above the fluorescence maximum (Fig. 3C). Ocean Station Papa (OSP, Station 8) contained the highest concentrations of labile Ni throughout the water column (Fig. 4C), and especially high labile Ni in surface waters relative to the other stations (Fig. 2C, 3C).

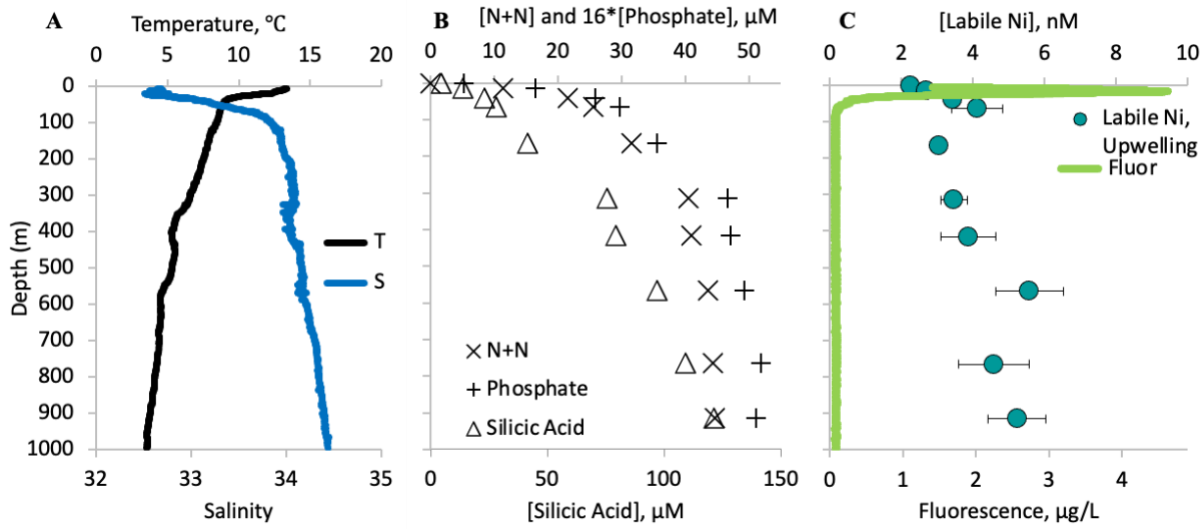

Figure 2. Depth profiles for station 1 sampled in the Northeast Pacific. Panel A shows temperature (top axis, black line) and salinity (bottom axis, blue line), panel B shows macronutrient concentrations, and panel C shows labile dissolved Ni concentrations (colored dots) and fluorescence (green line).

Concentrations of macronutrients (N+N, phosphate, and silicic acid) were drawn down to zero or near-zero at all stations except for Station 8, Ocean Station Papa (Fig. 4B, S3-O). Distributions of these macronutrients followed roughly the same shape within a single profile in the upper 275 m. Concentrations of labile Ni typically tracked well with N+N (hereafter, simply nitrate due to negligible nitrite concentrations) in the upper 500 m of the depth profiles (Fig. 2B, 3B, 4B and 2C, 3C, 4C), though there was a decoupling of labile Ni and nitrate in waters shallower than 100 m, except for Station 1 (Fig. 3B and 3C). Below 500 m, labile Ni tracked more closely with silicic acid until the deepest depths of the profiles, where labile Ni concentrations decoupled from silicic acid due to large decreases in labile Ni relative to silicic acid (Fig. 2B, 3B, 4B and 2C, 3C, 4C). Labile Ni concentrations were highest at depth,

approaching 8 nM in the 800 m samples of most stations, and in the 450-550 m samples of Stations 1 and 3 (Fig. S3-B and 3-F). In general, the deepest two depths generally saw the most variation in waters > 500 m, with the exception of Station 3 (Fig. S3-F).

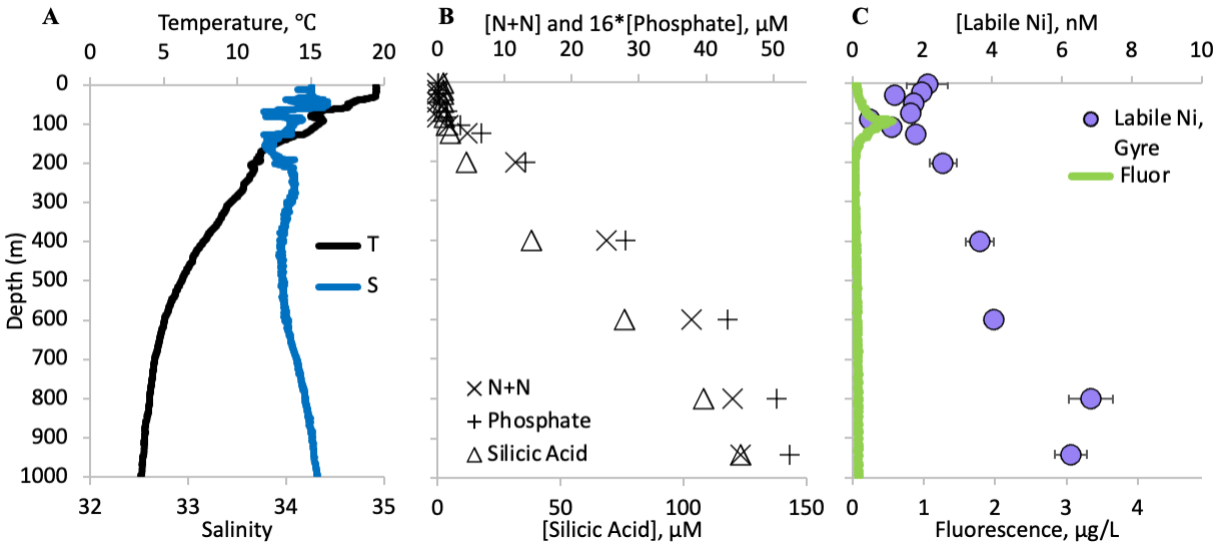

Figure 3. Depth profiles for station 5 sampled in the Northeast Pacific. Panel A shows temperature (top axis, black line) and salinity (bottom axis, blue line), panel B shows macronutrient concentrations, and panel C shows labile dissolved Ni concentrations (colored dots) and fluorescence (green line).

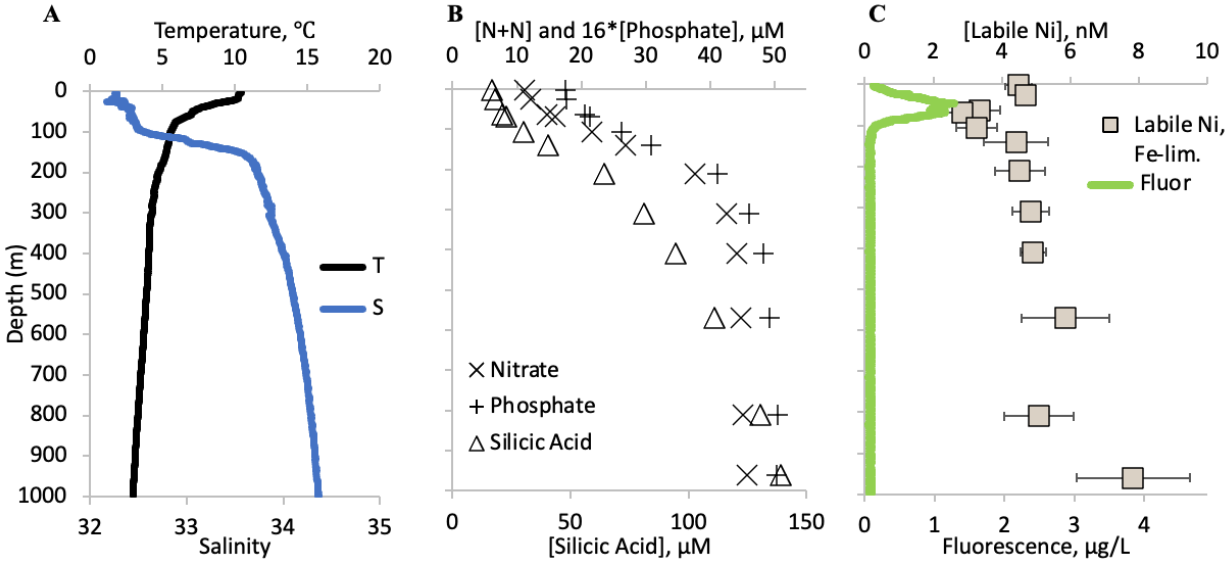

Figure 4. Depth profiles for station 8 sampled in the Northeast Pacific. Panel A shows temperature (top axis, black line) and salinity (bottom axis, blue line), panel B shows macronutrient concentrations, and panel C shows labile dissolved Ni concentrations (colored dots) and fluorescence (green line).

Overall, macronutrient concentrations tracked more closely with apparent oxygen utilization (AOU) through the water column profiles than labile dissolved Ni (Fig. 5, 6, 7, S5). In

the deepest waters with the highest potential densities, AOU and macronutrient concentrations were highest. Labile Ni concentrations, on the other hand, appeared to be lower in the deepest waters by a margin of 0.5-2.5 nM than would be expected following AOU and macronutrient trends at depth (Fig. 5B, 6B, 7B). This discrepancy of lower labile Ni at depth was observed in a water mass characterized by potential densities (σ_θ) of 25.5 – 26.5 kg m^{-3}.

Trends in labile Ni vs. macronutrient/apparent oxygen utilization (AOU) had R^2 values at or above 0.72 across all plots (Fig. 8). There was a distinct clustering of data at the low and high concentrations across all plots except for silicic acid (Fig. 8D), which had the majority of data clustered at the lowest concentrations, generally < 10 µM. Excursions outside the 1-to-1 line also occurred for all variables and were most prominent for Stations 1, 2, and 8 (Fig. 8).

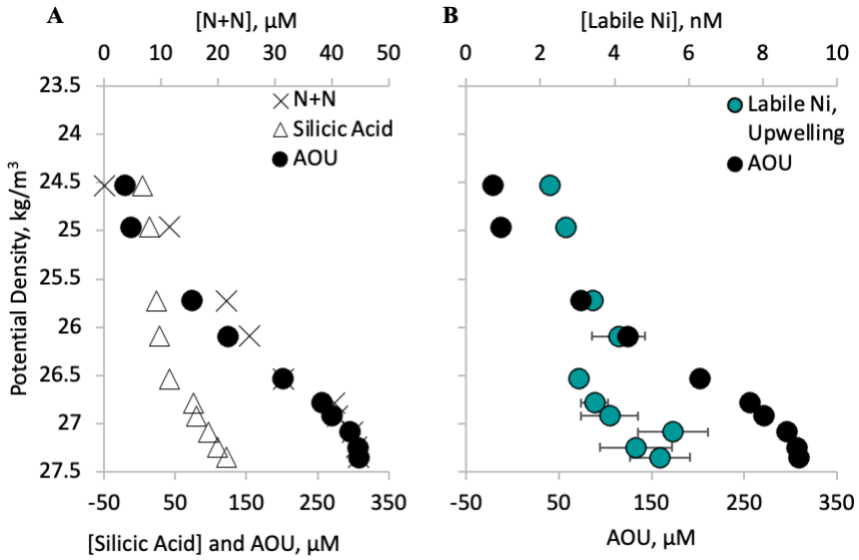

Figure 5. Potential density profiles for station 1 sampled in the Northeast Pacific. Panel A shows macronutrient concentrations and AOU (apparent oxygen utilization), and panel B shows labile dissolved Ni concentrations (colored dots) and AOU (black dots).

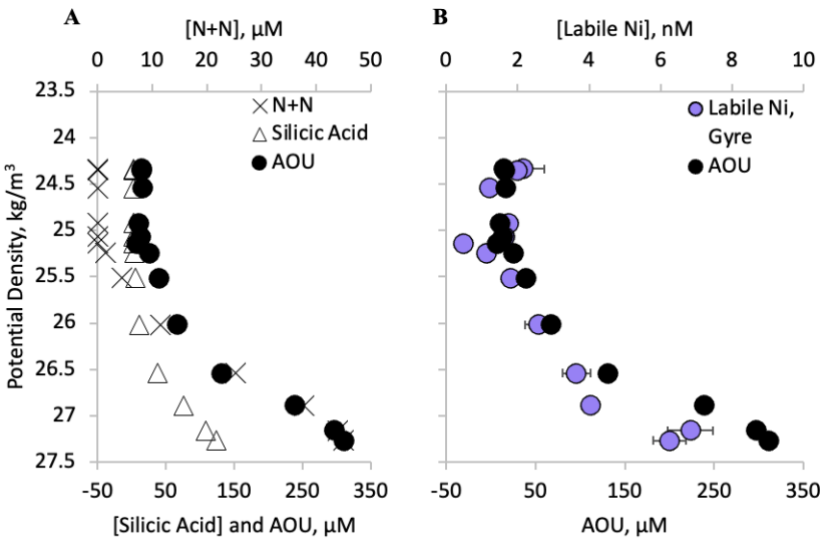

Figure 6. Potential density profiles for station 5 sampled in the Northeast Pacific. Panel A shows macronutrient concentrations and AOU (apparent oxygen utilization), and panel B shows labile dissolved Ni concentrations (colored dots) and AOU (black dots).

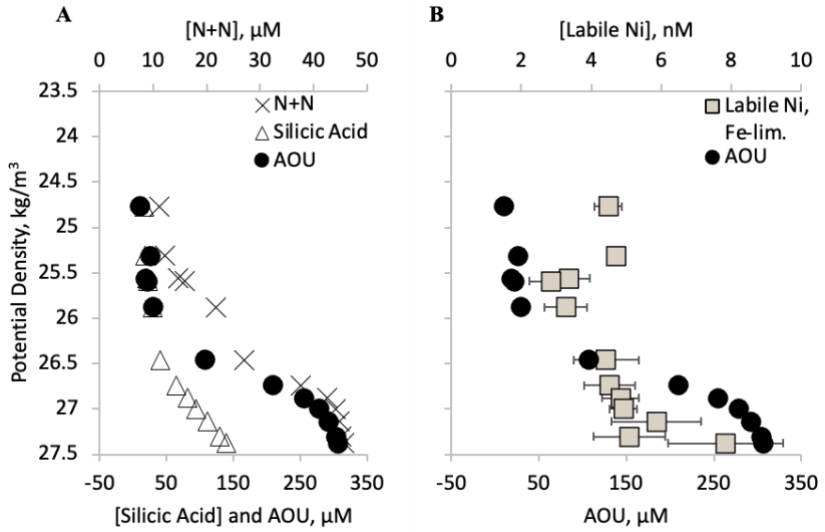

Figure 7. Potential density profiles for station 5 sampled in the Northeast Pacific. Panel A shows macronutrient concentrations and AOU (apparent oxygen utilization), and panel B shows labile dissolved Ni concentrations (colored dots) and AOU (black dots).

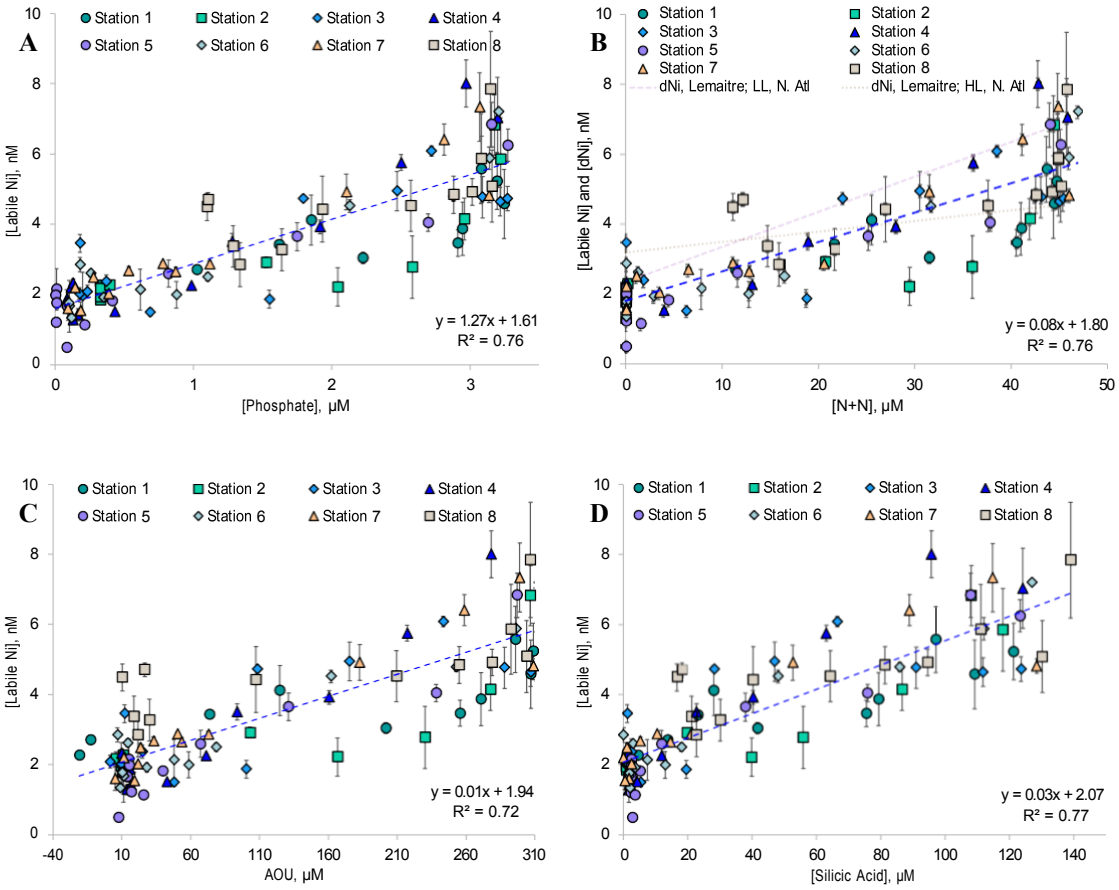

Figure 8. Labile dissolved Ni vs. macronutrient concentrations or apparent oxygen utilization (AOU) for all stations. Error bars represent one standard deviation of the average labile dissolved Ni from triplicate measurements. The dashed blue lines and accompanying equations represent the best-fit lines for all data from this study; additional dashed and dotted lines in the nitrate+nitrite (N+N) panel (B) are from Lemaitre et al. 2022 for total dissolved (rather than labile dissolved) Ni concentrations in the low and high latitude North Atlantic, respectively.

Discussion

Nutrient-like profiles of labile Ni

Labile dissolved Ni profiles in this study were nutrient-like, with lower concentrations in the upper water column and higher concentrations at depth. However, there were also substantial departures from classic nutrient-type profiles in the labile Ni distributions. Mixed layer depths based on temperature and salinity profiles (Fig. S2) ranged from 5 to 40 m across the eight stations. Labile Ni concentrations in these mixed layers varied, but were always higher than 1.5 nM (Table 1, Fig. S4). Stations 5 and 8 had surface maxima in labile Ni (Fig. 3 and 4C), where

dNi concentrations such as those from Bruland, 1980 (Fig. S1) are typically at a minimum. Station 5, which exhibited a surface maximum (Fig. 3C) was also one of the stations with the deepest mixed layer depth, along with Station 4, which were both oligotrophic (Fig. S2-H, J). Within the euphotic zone, an increase in the proportion of labile to dNi at the surface may reflect photochemical degradation of organic Ni-binding ligands. This process would increase labile Ni by converting organically complexed dissolved Ni (NiL) to labile Ni (Ni') species. Photochemical degradation of metal-binding organic ligands has been observed for iron (Barbeau 2006; Hassler et al. 2020) and other trace metals (Moffett 1995; Mellett and Buck 2020) in the open ocean. However, the photoreactivity of Ni-binding organic ligands in seawater has not been tested.

Table 1. Concentrations of averaged labile dissolved Ni and nitrate+nitrite (N+N) concentrations for the mixed layer depth (MLD) samples of each station.

Station	MLD, m	Avg. labile Ni, nM	Avg. N+N, μM
1	25	2.5 ± 0.1 (n=2)	5.7
2	30	1.9 ± 0.1 (n=3)	<LOD
3	25	2.7 ± 0.5 (n=2)	<LOD
4	40	1.8 ± 0.2 (n=3)	<LOD
5	40	1.8 ± 0.2 (n=3)	<LOD
6	25	2.3 ± 0.5 (n=2)	<LOD
7	5	1.6 ± 0.3 (n=1)	<LOD
8	26	4.6 ± 0.3 (n=2)	11.7

Concentrations of N+N that were below the limit of detection of the analyses (<0.03 μM) are denoted using <LOD. Errors represent one standard deviation of averaged results; n values represent the number of samples averaged from within the MLD, each of which was analyzed in triplicate.

Station 8 (OSP) exhibited a completely different distribution pattern with high surface labile Ni concentrations potentially reflecting a source from winter mixing remaining in the macronutrient-replete but Fe-limited surface waters. This surface maximum was even more prominent when compared to the pronounced minimum at the subsurface fluorescence maximum (Fig. 4C). Ocean Station Papa is an Fe-limited station in the high macronutrient lower than

expected chlorophyll (HNLC) regime of the subarctic North Pacific (Martin and Fitzwater 1988), and correspondingly had the highest surface water macronutrient concentrations (Fig. 4B; Table 1). The growth of large diatoms is limited by Fe in these waters, but small phytoplankton including *Synechococcus* and autotrophic flagellates are found in surface waters and through the upper 60 m of the water column (Boyd and Harrison 1999). Notably, the macronutrient-rich conditions of these waters did not appear to support more Ni drawdown by these smaller phytoplankton here compared to the more oligotrophic stations as might be expected from culture studies (John et al. 2022), and a minimum in labile Ni was only observed ~20 m below the subsurface fluorescence maximum (Fig. 4C).

The observed minima in labile dissolved Ni concentrations associated with fluorescence maxima of most stations suggested that dNi is indeed bioavailable. In many of these profiles, the minima in labile Ni occurred at the same depth as the fluorescence maxima, more directly linking the drawdown of labile Ni with biomass accumulation. In the profiles of other stations, however, labile Ni drawdown was more evident within the first 100 m below the fluorescence maxima. In all stations except the coastal upwelling station (Station 1), the localized upper water column minima in labile dissolved Ni were in subsurface waters (Fig. S4). This was surprising since demand for Ni is expected to be highest in surface waters, where dissolved organic nitrogen species like urea are a more abundant component of the nitrogen pool and where higher light intensities would increase demand for cellular SOD. The lack of labile Ni drawdown in surface waters may also reflect a rapid turnover cycle of Ni and photochemical maintenance of labile Ni in surface waters rather than an absence of demand. Deeper in the euphotic zone, scavenging of regenerated dissolved Ni to manganese (Mn) oxides or heterotrophic Ni uptake may contribute to the subsurface minimum in labile Ni.

At depth, dissolved Ni (dNi) has been shown to exhibit dual regeneration patterns with phosphate and with silicic acid (Bruland 1980; Twining et al. 2012). In these profiles, there was also evidence for similar shallow and deep regeneration cycles. Station 1 and 2 had shallow water maxima in labile Ni concentrations within 80 m below the fluorescence maxima (Fig. S4-B, S4-D), alongside increased macronutrient concentrations (Fig. S4-A, S4-C), indicative of organic matter regeneration. Labile dissolved Ni concentrations in stations 3-7 tracked well with nitrate outside of the mixed layer and above 150 m (Fig. S4), also consistent with remineralization. At intermediate depths, the decoupling of labile Ni concentrations from macronutrients may suggest a loss of labile Ni in these waters via heterotrophic demand or scavenging to Mn oxides. A recent proteomic study uncovered a possible contribution to labile Ni drawdown where marine heterotrophs utilized Ni to metabolize glucose (Mazzotta et al. 2021). In addition, dark incubation studies have presented evidence of delayed regeneration of Ni from decaying diatoms tied to Mn oxidation (Hollister et al. 2020). Manganese and Ni were also coupled in incubation studies of the California Current as Ni drawdown in dark experiments was attributed to scavenging onto Mn-oxides (Mellett et al. 2018), which may lead to irreversible structural incorporation in Mn particles (Peacock and Sherman 2007). The preferential scavenging of Ni to Mn-oxides may therefore serve as an important sink of dissolved and labile Ni below the euphotic zone.

In the deepest two to three depths of all profiles, there was a negative offset between Ni and macronutrients, with nitrate and silicic acid concentrations increasing in tandem with AOU but a decline in labile Ni (Fig. S5). Figure S5 shows AOU, macronutrient concentrations, and labile Ni concentrations plotted against potential density, to better compare water masses across the stations. Previous studies have published the salinity ranges for Antarctic Intermediate Water

(AAIW) and North Pacific Intermediate Water (NPIW) of 34.4–34.6 (Tomczak and Godfrey 1994; Behrens et al. 2018) and 34.0–34.3 (Behrens et al. 2018), respectively. When compared to the salinity range of water below 300 m for these data ~34.0 - 34.4 (Fig. 2), the lower end of the AAIW range falls on the upper range for these profiles. In contrast, the range for NPIW encompasses these data well, with small excursions outside of the published range. Similarly, the density ranges from these same publications for AAIW and NPIW were 26.8–27.3 and 26.6–27.4, respectively. When considering the density range for the low concentrations of labile dissolved Ni of 26.5-27.5 for this study, the NPIW range encompasses these more completely (Fig 2, Fig. 5). Previously published data from Bruland (1980) show total dissolved Ni (dNi) concentrations that are either maintained or which increase at depth (Fig. S1).

The decoupling of the dNi from the labile Ni data seems to signify that the water mass of NPIW present in these samples has a fundamentally different Ni chemistry (Fig. S1) where less of the dNi is composed of labile species in waters with the highest AOU. Since AOU reflects the respiration of organic matter in waters separated from the atmosphere, we expect this water mass to have the longest isolation from the surface. The density plots of AOU, labile Ni, and macronutrients (Fig. 5-7) show lower concentrations of labile Ni in waters with the highest AOU. Below the 26.5 kg m^{-3} isopycnal, there was a negative offset in labile Ni concentrations compared to AOU for all stations except those in the oligotrophic gyre, with a muted increase in labile Ni relative to AOU (Stations 4-6, Fig. S5-H, J, L). Furthermore, stations 1 and 8 showed a decline in labile dissolved Ni with increasing AOU. These low labile Ni values are not consistent with the previously observed release of total dissolved Ni at depth (Bruland 1980). A decline in labile dissolved Ni concurrent with an increase in dNi concentrations would suggest a transformation of labile Ni to non-labile Ni within the dNi pool in these aged deep waters.

Labile Ni-macronutrient relationships

Through much of the profiles, labile Ni, N+N (nitrate), phosphate, and AOU were consistent with release of labile Ni from organic matter respiration (Fig. 8). When compared with nitrate, the best fit lines from Lemaitre et al. 2022, for the low (pink dashed) and high (dotted) latitude North Atlantic compared well with our lower (Stations 1-7) and higher (Station 8, OSP) latitude station labile Ni concentrations (Fig. 8B). The dissolved Ni data fit for the low latitude North Atlantic roughly paralleled the line of best fit for our data (blue dashed). Labile Ni concentration relationships with phosphate (Fig. 8A) and nitrate (Fig. 8B) were similar and reasonably well correlated at the lower end of the concentration scale, consistent with labile Ni incorporation in organic matter production and remineralization in the upper water column. At higher concentrations of macronutrients, labile Ni had a closer relationship with silicic acid (Fig. 8D), consistent with a secondary remineralization signal associated with the release of Ni from diatom frustules at depth (Bruland 1980; Twining et al. 2012).

One of the key differences between the high latitude North Atlantic and North Pacific is the pronounced Fe limitation of large phytoplankton growth in surface waters of the subarctic North Pacific (Martin and Fitzwater 1988). In surface waters of Ocean Station Papa (Station 8, this study), macronutrient concentrations were higher than the other stations sampled, and labile Ni concentrations in these waters were not only higher than the other stations (Fig. 3, Fig. 4), but were also higher than subsurface waters with similar macronutrient concentrations (Fig. 7). Station 1, in an aging coastal upwelling plume that became Fe limited (shipboard incubation data not shown), also had elevated labile Ni concentrations in surface waters despite evidence for high productivity, including elevated biomass fluorescence, declining macronutrient concentrations, and negative AOU (Fig. 5A, B). Previous studies of labile Ni in open ocean

surface waters also reported elevated labile Ni contributions to the dNi pool in Fe-limited surface waters (Saito et al. 2004; Boiteau et al. 2016). Altogether, these data suggest that Fe limitation also limits the biological uptake of labile Ni, and that large diatoms play a major role in the cycling of Ni (Twining et al. 2012).

Effects of pH on labile Ni measurements

In this study, samples were accidentally buffered to pH 9.0. However, the binding capacity of DMG for the $Ni(DMG)_2$ complex and labile dissolved Ni measurements has only been calibrated at pH 8.4 (van den Berg and Nimmo 1987), and the only other studies of labile dissolved Ni with this method have applied it at pH 7.8-8.1 using an organic EPPS buffer (Donat et al. 1994; Saito et al. 2004; Boiteau et al. 2016). To our knowledge, the measurement of labile Ni with DMG has never been tested as a function of pH. However, a very similar method that uses DMG to measure labile dissolved cobalt (Co) has been calibrated as a function of seawater pH over the range of pH 7.0 to 8.5 (Saito and Moffett 2001).The results of that study found that the conditional stability constant for the $Co(DMG)_2$ complex, which averaged $10^{11.5 \pm 0.3}$ at pH 8.0, increased by 1 log unit for every 0.5 pH unit increase. If the conditional stability constant for $Ni(DMG)_2$ behaves similarly as a function of pH, then the higher pH of our analyses would have led to stronger competition for dNi by the added DMG, and we may have overestimated the concentrations of labile dissolved Ni for this study. This may preclude these data from being directly comparable to other studies of labile Ni, though the surface concentrations from this study still fall within the expected range from previous studies (Saito et al. 2004; Boiteau et al. 2016) and the concentration of labile dissolved Ni in some of our subsurface maxima were very low (Fig. 3 and 4C). Nevertheless, until further investigations establish the role of pH in these measurements, our data should only be compared internally; the same pH buffering and

corresponding operationally defined measurement of labile dissolved Ni was applied across all samples in this study.

Conclusions

This study presents the first depth profiles of labile dissolved Ni concentrations in the oceans to date. Depth profiles revealed that labile Ni behaves generally like dissolved Ni (dNi), a nutrient-type element, with several notable distinctions. The lowest concentrations of labile Ni were associated with subsurface fluorescence maxima. Surface maxima in labile Ni concentrations where dNi concentrations are typically at a minimum suggest that photochemical degradation of organically complexed dNi may be an important source of labile Ni in surface waters. The highest concentrations of labile Ni in surface waters were observed when large diatom communities were Fe limited, reflecting the importance of diatoms in Ni cycling. Deeper in the profiles, maxima in labile Ni concentrations were found associated with dual regeneration cycles, consistent with previous findings of shallow (< 800 m) and deep (≥ 800 m) regeneration cycles of dNi associated with phosphate/nitrate and silicic acid, respectively. Anomalously low labile dissolved Ni relative to macronutrients at intermediate depths may suggest preferential scavenging onto Mn oxides or heterotrophic Ni demand. In samples where labile Ni concentrations decreased relative to macronutrients and apparent oxygen utilization (generally ≥ 800 m), decreases in dNi were not evident in previously published data. A loss of labile Ni but not dNi may reflect a change in the speciation of dNi in deep waters over time. These data provide important insights into the cycling and bioavailability of dNi, an understudied trace metal micronutrient in the marine environment.

References Cited

Antia, N. J., B. R. Berland, D. J. Bonin, and S. Y. Maestrini. 1975. Comparative evaluation of certain organic and inorganic sources of nitrogen for phototrophic growth of marine microalgae. Journal of the Marine Biological Association of the United Kingdom **55**: 519–539.

Barbeau, K. 2006. Photochemistry of organic iron (III) complexing ligands in oceanic systems. Photochemistry and Photobiology **82**: 1505–1516. doi:10.1562/2006-06-16-IR-935

Bedsworth, W. W., and D. L. Sedlak. 1999. Sources and environmental fate of strongly complexed nickel in estuarine waters: The role of ethylenediaminetetraacetate. Environmental Science & Technology **33**: 926–931. doi:10.1021/es9809556

Behrens, M. K., K. Pahnke, B. Schnetger, and H.-J. Brumsack. 2018. Sources and processes affecting the distribution of dissolved Nd isotopes and concentrations in the West Pacific. Geochimica et Cosmochimica Acta **222**: 508–534. doi:10.1016/j.gca.2017.11.008

Boiteau, R. M., C. P. Till, A. Ruacho, and others. 2016. Structural characterization of natural nickel and copper binding ligands along the US GEOTRACES Eastern Pacific zonal transect. Frontiers in Marine Science **3**. doi:10.3389/fmars.2016.00243

Boyd, P., and P. J. Harrison. 1999. Phytoplankton dynamics in the NE subarctic Pacific. Deep Sea Research Part II: Topical Studies in Oceanography **46**: 2405–2432. doi:10.1016/S0967-0645(99)00069-7

Boyle, E. A., S. S. Huested, and S. P. Jones. 1981. On the distribution of copper, nickel, and cadmium in the surface waters of the North Atlantic and North Pacific Ocean. Journal of Geophysical Research **86**: 8048. doi:10.1029/JC086iC09p08048

Bruland, K. W. 1980. Oceanographic distributions of cadmium, zinc, nickel, and copper in the North Pacific. Earth and Planetary Science Letters **47**: 176–198. doi:10.1016/0012-821X(80)90035-7

Bruland, K. W., and R. P. Franks. 1983. Mn, Ni, Cu, Zn and Cd in the Western North Atlantic, p. 395–414. *In* C.S. Wong, E. Boyle, K.W. Bruland, J.D. Burton, and E. Goldberg [eds.], Trace Metals in Sea Water.

Cutter, G., K. Casciotti, P. Croot, W. Geibert, L.-E. Heimbürger, M. Lohan, H. Planquette, and T. van de Flierdt. 2017. GEOTRACES sampling protocol cookbook, version 3.0.

Donat, J. R., K. A. Lao, and K. W. Bruland. 1994. Speciation of dissolved copper and nickel in South San Francisco Bay A multi-method approach. Analytica Chimica Acta **284**: 547–571. doi:10.1016/0003-2670(94)85061-5

Dupont, C. L., K. N. Buck, B. Palenik, and K. Barbeau. 2010. Nickel utilization in phytoplankton assemblages from contrasting oceanic regimes. Deep Sea Research Part I: Oceanographic Research Papers **57**: 553–566. doi:10.1016/j.dsr.2009.12.014

Dupont, C. L., K. Neupane, J. Shearer, and B. Palenik. 2008. Diversity, function and evolution of genes coding for putative Ni-containing superoxide dismutases. Environmental Microbiology **10**: 1831–1843. doi:10.1111/j.1462-2920.2008.01604.x

Fridovich, I. 1997. Superoxide anion radical (O_2^-), superoxide dismutases, and related matters. Journal of Biological Chemistry **272**: 18515–18517. doi:10.1074/jbc.272.30.18515

Gledhill, M., and K. N. Buck. 2012. The organic complexation of iron in the marine environment: A review. Frontiers in Microbiology **3**. doi:10.3389/fmicb.2012.00069

Gordon, L., J. Jennings, A. Ross, and J. Krest. 1993. A suggested protocol for continuous flow automated analysis of seawater nutrients (phosphate, nitrate, nitrite and silicic acid) in the WOCE hydrographic program and the joint global ocean fluxes study. Methods Manual WHPO **91–1**.

Hassler, C., D. Cabanes, S. Blanco-Ameijeiras, S. G. Sander, and R. Benner. 2020. Importance of refractory ligands and their photodegradation for iron oceanic inventories and cycling. Marine and Freshwater Research **71**: 311. doi:10.1071/MF19213

Ho, T.-Y. 2013. Nickel limitation of nitrogen fixation in *Trichodesmium*. Limnology and Oceanography **58**: 112–120. doi:10.4319/lo.2013.58.1.0112

Hollister, A. P., M. Kerr, K. Malki, and others. 2020. Regeneration of macronutrients and trace metals during phytoplankton decay: An experimental study. Limnology and Oceanography **65**: 1936–1960. doi:10.1002/lno.11429

John, S. G., R. L. Kelly, X. Bian, and others. 2022. The biogeochemical balance of oceanic nickel cycling. Nature Geoscience **15**: 906–912. doi:10.1038/s41561-022-01045-7

Lemaitre, N., J. H. Du, G. F. de Souza, C. Archer, and D. Vance. 2022. The essential bioactive role of nickel in the oceans: Evidence from nickel isotopes. Earth and Planetary Science Letters **584**: 11. doi:10.1016/j.epsl.2022.117513

Mackey, D. J., J. E. O'Sullivan, R. J. Watson, and G. Dal Pont. 2002. Trace metals in the Western Pacific: temporal and spatial variability in the concentrations of Cd, Cu, Mn and Ni. Deep-Sea Research Part I **49**: 2241–2259. doi:10.1016/s0967-0637(02)00124-3

Martin, J. H. 1990. Glacial-interglacial CO_2 change: The iron hypothesis. Paleoceanography **5**: 1–13. doi:10.1029/PA005i001p00001

Martin, J. H., and S. Fitzwater. 1988. Iron-deficiency limits phytoplankton growth in the northeast pacific subarctic. Nature **331**: 341–343. doi:10.1038/331341a0

Mazzotta, M. G., M. R. McIlvin, D. M. Moran, D. T. Wang, K. D. Bidle, C. H. Lamborg, and M. A. Saito. 2021. Characterization of the metalloproteome of *Pseudoalteromonas* (BB2-AT2): biogeochemical underpinnings for zinc, manganese, cobalt, and nickel cycling in a ubiquitous marine heterotroph. Metallomics **13**: mfab060. doi:10.1093/mtomcs/mfab060

Mellett, T., M. T. Brown, P. D. Chappell, and others. 2018. The biogeochemical cycling of iron, copper, nickel, cadmium, manganese, cobalt, lead, and scandium in a California Current experimental study. Limnology and Oceanography **63**: S425–S447. doi:10.1002/lno.10751

Mellett, T., and K. N. Buck. 2020. Spatial and temporal variability of trace metals (Fe, Cu, Mn, Zn, Co, Ni, Cd, Pb), iron and copper speciation, and electroactive Fe-binding humic substances in surface waters of the eastern Gulf of Mexico. Marine Chemistry **227**. doi:10.1016/j.marchem.2020.103891

Moffett, J. W. 1995. Temporal and spatial variability of copper complexation by strong chelators in the Sargasso Sea. Deep Sea Research Part I **42**: 1273–1295. doi:10.1016/0967-0637(95)00060-J

Moore, C. M., M. M. Mills, K. R. Arrigo, and others. 2013. Processes and patterns of oceanic nutrient limitation. Nature Geoscience **6**: 701–710. doi:10.1038/ngeo1765

Moore, J. K., S. C. Doney, D. M. Glover, and I. Y. Fung. 2001. Iron cycling and nutrient-limitation patterns in surface waters of the World Ocean. Deep Sea Research Part II **49**: 463–507. doi:https://doi.org/10.1016/S0967-0645(01)00109-6

Omanović, D., C. Garnier, and I. Pižeta. 2015. ProMCC: An all-in-one tool for trace metal complexation studies. Marine Chemistry **173**: 25–39. doi:10.1016/j.marchem.2014.10.011

Parsons, T. R., Y. Maita, and C. M. Lalli. 1984. A manual of chemical and biological methods for seawater analysis, Pergamon.

Peacock, C. L., and D. M. Sherman. 2007. Crystal-chemistry of Ni in marine ferromanganese crusts and nodules. American Mineralogist **92**: 1087–1092. doi:10.2138/am.2007.2378

Pihlar, B., P. Valenta, and H. W. Nürnberg. 1981. New high-performance analytical procedure for the voltammetric determination of nickel in routine analysis of waters, biological materials and food. Fresenius' Zeitschrift für analytische Chemie **307**: 337–346. doi:10.1007/BF00480109

Price, N. M., and F. M. M. Morel. 1991. Colimitation of phytoplankton growth by nickel and nitrogen. Limnology and Oceanography **36**: 1071–1077. doi:10.4319/lo.1991.36.6.1071

Qiu, B. S., and N. M. Price. 2009. Different physiological responses of four marine *Synechococcus* strains (Cyanophyceae) to nickel starvation under iron-replete and iron-deplete conditions. Journal of Phycology **45**: 1062–1071. doi:10.1111/j.1529-8817.2009.00732.x

Saito, M. A., and J. W. Moffett. 2001. Complexation of cobalt by natural organic ligands in the Sargasso Sea as determined by a new high-sensitivity electrochemical cobalt speciation method suitable for open ocean work. Marine Chemistry **75**: 49–68. doi:10.1016/s0304-4203(01)00025-1

Saito, M. A., J. W. Moffett, and G. R. DiTullio. 2004. Cobalt and nickel in the Peru upwelling region: A major flux of labile cobalt utilized as a micronutrient. Global Biogeochemical Cycles **18**: GB4030. doi:10.1029/2003gb002216

Sclater, F. R., E. Boyle, and J. M. Edmond. 1976. On the marine geochemistry of nickel. Earth and Planetary Science Letters **31**: 119–128. doi:https://doi.org/10.1016/0012-821X(76)90103-5

Strickland, J. D. H., and T. R. Parsons. 1972. A Practical Handbook of Seawater Analysis, 2nd ed. Fisheries Research Board of Canada.

Sunda, W. G. 1989. Trace metal interactions with marine phytoplankton. Biological Oceanography **6**: 411–442. doi:10.1080/01965581.1988.10749543

Tomczak, M., and J. S. Godfrey. 1994. Chapter 9 - Hydrology of the Pacific Ocean, p. 149–171. *In* M. Tomczak and J.S. Godfrey [eds.], Regional Oceanography. Pergamon.

Twining, B. S., S. B. Baines, S. Vogt, and D. M. Nelson. 2012. Role of diatoms in nickel biogeochemistry in the ocean. Global Biogeochemical Cycles **26**: 9. doi:10.1029/2011gb004233

Van den Berg, C. M. G., and M. Nimmo. 1987. Determination of interactions of nickel with dissolved organic material in seawater using cathodic stripping voltammetry. Science of the Total Environment **60**: 185–195. doi:10.1016/0048-9697(87)90415-3

Appendix A: Data Tables

Table S1. Table of hydrographic data from this study.

Station	Date	Latitude deg N	Longitude deg E	Density kg/m^3	Depth m	Salinity	Temperature deg C	Oxygen µM
1	6/9/22	40.111	-125.563	24.5339	2	32.67	13.29	281.42
1	6/9/22	40.111	-125.563	24.9631	15	32.66	10.97	286.29
1	6/9/22	40.111	-125.563	25.7248	40	33.21	8.95	211.32
1	6/9/22	40.111	-125.563	26.0908	65	33.62	8.66	161.19
1	6/9/22	40.111	-125.563	26.5339	165	33.99	7.63	90.11
1	6/9/22	40.111	-125.563	26.7812	315	34.08	6.39	44.62
1	6/9/22	40.111	-125.563	26.9182	415	34.14	5.65	34.45
1	6/9/22	40.111	-125.563	27.083	565	34.18	4.52	17.80
1	6/9/22	40.111	-125.563	27.2452	765	34.34	4.23	8.35
1	6/9/22	40.111	-125.563	27.3488	915	34.40	3.70	10.69
2	6/12/22	38.824	-130.511	24.0109	2	32.61	15.54	239.71
2	6/12/22	38.824	-130.511	24.147	15	32.61	14.93	239.86
2	6/12/22	38.824	-130.511	24.4339	29	32.64	13.66	244.44
2	6/12/22	38.824	-130.511	24.4767	42	32.63	13.41	254.27
2	6/12/22	38.824	-130.511	24.6351	65	32.64	12.64	253.09
2	6/12/22	38.824	-130.511	25.7862	155	33.35	9.29	179.34
2	6/12/22	38.824	-130.511	26.5231	264	33.94	7.44	126.49
2	6/12/22	38.824	-130.511	26.7197	363	34.05	6.69	67.91
2	6/12/22	38.824	-130.511	26.9939	560	34.10	4.74	34.34
2	6/12/22	38.824	-130.511	27.2028	760	34.28	4.15	9.42
2	6/12/22	38.824	-130.511	27.3082	908	34.37	3.84	8.40
3	6/13/22	37.802	-134.423	23.9581	2	33.04	17.24	230.63
3	6/13/22	37.802	-134.423	24.0737	21	33.03	16.71	230.72
3	6/13/22	37.802	-134.423	24.6704	50	33.17	14.49	243.84
3	6/13/22	37.802	-134.423	24.5455	75	32.86	13.95	255.28
3	6/13/22	37.802	-134.423	24.914	100	33.08	12.99	236.45
3	6/13/22	37.802	-134.423	25.4199	140	33.31	11.23	222.86
3	6/13/22	37.802	-134.423	26.1022	200	33.75	9.25	181.46
3	6/13/22	37.802	-134.423	26.3944	249	33.90	8.11	180.33

Table S1 (Continued).

3	6/13/22	37.802	-134.423	26.6279	349	33.94	6.70	122.95
3	6/13/22	37.802	-134.423	26.8049	448	34.01	5.75	61.37
3	6/13/22	37.802	-134.423	27.0318	616	34.14	4.72	24.30
3	6/13/22	37.802	-134.423	27.205	795	34.27	4.02	10.19
3	6/13/22	37.802	-134.423	27.3215	943	34.37	3.69	8.21
4	6/14/22	36.741	-138.392	24.0067	2	33.35	18.02	220.58
4	6/14/22	36.741	-138.392	24.0423	21	33.36	17.90	223.13
4	6/14/22	36.741	-138.392	24.0629	31	33.36	17.80	224.92
4	6/14/22	36.741	-138.392	24.6596	61	33.83	16.81	231.48
4	6/14/22	36.741	-138.392	24.7876	75	33.58	15.43	237.94
4	6/14/22	36.741	-138.392	24.9129	101	33.48	14.48	236.29
4	6/14/22	36.741	-138.392	25.3413	151	33.56	12.71	219.49
4	6/14/22	36.741	-138.392	25.8698	202	33.69	10.38	203.77
4	6/14/22	36.741	-138.392	26.3269	302	33.98	8.97	189.53
4	6/14/22	36.741	-138.392	26.5598	402	33.97	7.41	132.77
4	6/14/22	36.741	-138.392	26.7968	502	34.00	5.77	87.57
4	6/14/22	36.741	-138.392	27.0531	701	34.12	4.34	36.84
4	6/14/22	36.741	-138.392	27.2817	948	34.30	3.54	9.37
5	6/16/22	35	-145	24.3362	2	34.26	19.47	213.57
5	6/16/22	35	-145	24.3523	21	34.26	19.41	213.40
5	6/16/22	35	-145	24.5416	30	34.36	18.98	213.69
5	6/16/22	35	-145	24.9204	51	34.47	17.74	225.47
5	6/16/22	35	-145	25.0665	75	33.85	15.08	235.27
5	6/16/22	35	-145	25.1404	90	34.14	15.77	237.87
5	6/16/22	35	-145	25.2419	110	34.01	14.88	224.30
5	6/16/22	35	-145	25.5146	130	33.88	13.07	219.68
5	6/16/22	35	-145	26.014	202	34.05	11.17	202.63
5	6/16/22	35	-145	26.5378	401	33.96	7.47	161.94
5	6/16/22	35	-145	26.888	600	34.00	5.02	71.90
5	6/16/22	35	-145	27.1558	800	34.20	4.01	20.30
5	6/16/22	35	-145	27.2675	941	34.29	3.57	9.95
6	6/20/22	38.815	-145	23.9528	2	33.34	18.19	228.72
6	6/20/22	38.815	-145	24.3915	26	33.37	16.46	232.09
6	6/20/22	38.815	-145	24.4767	36	33.42	16.25	234.05
6	6/20/22	38.815	-145	25.0373	71	33.62	14.41	244.40
6	6/20/22	38.815	-145	25.1836	82	33.58	13.57	243.24
6	6/20/22	38.815	-145	25.2658	100	33.47	12.71	234.12
6	6/20/22	38.815	-145	25.6676	131	33.69	11.49	220.87
6	6/20/22	38.815	-145	26.0216	171	33.91	10.49	215.48

Table S1 (Continued).

6	6/20/22	38.815	-145	26.1905	211	34.00	9.93	198.81
6	6/20/22	38.815	-145	26.628	410	33.94	6.72	136.31
6	6/20/22	38.815	-145	26.9699	610	34.05	4.59	60.60
6	6/20/22	38.815	-145	27.1699	810	34.20	3.85	22.36
6	6/20/22	38.815	-145	27.2834	960	34.29	3.43	11.13
7	6/21/22	41.966	-145.001	24.1931	2	32.87	15.62	243.33
7	6/21/22	41.966	-145.001	24.6808	31	32.90	13.43	248.17
7	6/21/22	41.966	-145.001	24.9117	45	32.97	12.54	245.09
7	6/21/22	41.966	-145.001	25.0759	56	33.01	11.83	244.64
7	6/21/22	41.966	-145.001	25.2007	85	33.03	11.25	249.67
7	6/21/22	41.966	-145.001	25.3503	110	33.11	10.75	240.98
7	6/21/22	41.966	-145.001	25.8009	140	33.45	9.66	229.56
7	6/21/22	41.966	-145.001	26.0043	170	33.65	9.35	228.18
7	6/21/22	41.966	-145.001	26.2579	211	33.87	8.87	211.08
7	6/21/22	41.966	-145.001	26.6983	410	33.90	5.93	121.02
7	6/21/22	41.966	-145.001	26.9765	602	34.03	4.43	55.92
7	6/21/22	41.966	-145.001	27.1961	810	34.22	3.72	20.72
7	6/21/22	41.966	-145.001	27.3004	960	34.30	3.33	13.84
8	6/26/22	49.999	-145.021	24.7674	2	32.28	10.38	267.67
8	6/26/22	49.999	-145.021	25.3145	26	32.41	7.45	269.91
8	6/26/22	49.999	-145.021	25.5608	63	32.48	6.03	287.55
8	6/26/22	49.999	-145.021	25.5913	70	32.49	5.80	286.20
8	6/26/22	49.999	-145.021	25.8777	106	32.80	5.48	279.48
8	6/26/22	49.999	-145.021	26.4577	140	33.50	5.27	202.15
8	6/26/22	49.999	-145.021	26.7387	211	33.76	4.60	104.50
8	6/26/22	49.999	-145.021	26.8768	310	33.88	4.21	61.65
8	6/26/22	49.999	-145.021	26.9971	410	34.01	4.05	38.76
8	6/26/22	49.999	-145.021	27.1387	570	34.15	3.78	26.69
8	6/26/22	49.999	-145.021	27.3063	810	34.30	3.26	19.25
8	6/26/22	49.999	-145.021	27.3751	960	34.35	3.00	18.28

Table S2. Table of labile dissolved Ni and macronutrient concentrations from this study.

Station	Depth	[Labile dNi]	Std Dev	AOU	Chl-GFF	P	N+N	Si
	m	nM	nM	µM	µg/L	µM	µM	µM
1	2	2.26	0.04	-20.91	1.72	0.32	0.00	4.57
1	15	2.70	0.12	-12.70	1.99	1.03	11.41	13.76
1	40	3.42	0.08	73.56	0.21	1.62	21.53	23.06
1	65	4.12	0.71	124.70	0.07	1.85	25.51	28.12
1	165	3.04	0.16	201.78	0.02	2.23	31.49	41.67
1	315	3.46	0.37	255.55	0.01	2.91	40.51	75.50
1	415	3.87	0.76	270.86	0.01	2.95	40.97	79.29
1	565	5.57	0.94	295.82	0.01	3.08	43.62	97.12
1	765	4.58	0.98	307.10	0.01	3.25	44.36	109.19
1	915	5.23	0.81	308.73	0.01	3.20	44.65	121.32
2	2	1.96	0.20	9.35	0.11	0.34	0.00	0.95
2	15	1.85	0.14	12.25	0.12	0.33	0.00	0.91
2	29	1.93	0.03	14.20	0.18	0.33	0.00	0.97
2	42	2.16	0.20	5.70	0.24	0.33	0.00	0.99
2	65	2.27	0.11	11.02	0.38	0.39	0.18	1.38
2	155	2.91	0.15	103.09	0.01	1.53	20.69	19.73
2	264	2.22	0.54	166.73	0.01	2.04	29.46	39.83
2	363	2.78	0.89	230.23	0.01	2.58	35.96	55.89
2	560	4.14	0.59	277.80	0.00	2.96	41.86	86.58
2	760	6.82	0.86	306.76	0.00	3.18	44.37	108.15
2	908	5.85	1.18	310.01	-0.01	3.22	44.81	117.95
3	2	1.96	0.67	9.61	0.09	0.20	0.00	1.21
3	21	3.46	0.26	11.96	0.11	0.18	0.00	1.20
3	50	2.03	0.17	9.50	0.16	0.18	0.00	1.21
3	75	2.08	0.18	1.40	0.27	0.23	0.00	0.94
3	100	2.37	0.19	24.96	0.19	0.37	1.84	2.42
3	140	1.50	0.10	47.97	0.08	0.69	6.28	5.34
3	200	1.87	0.26	100.46	0.07	1.55	18.71	19.53
3	249	4.73	0.08	108.56	0.00	1.79	22.49	28.16
3	349	4.94	0.56	175.35	0.00	2.47	30.53	46.95
3	448	6.08	0.14	243.54	0.00	2.72	38.51	66.40
3	616	4.77	0.59	287.85	0.00	3.09	43.08	91.00
3	795	4.64	0.41	307.02	0.00	3.22	44.90	111.76
3	943	4.72	0.35	311.42	0.00	3.27	45.33	123.56
4	2	1.87	0.27	15.60	0.15	0.08	0.00	1.52
4	21	1.28	0.14	13.58	0.16	0.13	0.00	1.51
4	31	2.19	0.06	12.22	0.12	0.11	0.00	1.47
4	61	1.77	0.11	9.46	0.19	0.08	0.00	1.69
4	75	2.32	0.13	9.98	0.23	0.13	0.00	1.59
4	101	1.42	0.18	16.59	0.31	0.16	0.00	1.83
4	151	1.52	0.02	42.57	0.08	0.43	3.91	4.24

Table S2 (Continued).

4	202	2.25	0.03	71.30	0.01	0.98	13.12	11.81
4	302	3.50	0.24	93.65	0.00	1.28	18.87	22.71
4	402	3.92	0.20	160.61	0.00	1.92	28.03	40.21
4	502	5.75	0.23	217.20	0.01	2.50	36.04	63.01
4	701	8.00	0.67	278.29	0.00	2.97	42.75	95.70
4	948	7.03	1.14	311.57	0.00	3.20	45.74	124.17
5	2	2.15	0.59	14.90	0.09	0.01	0.00	2.45
5	21	1.98	0.08	15.34	0.09	0.00	0.00	2.42
5	30	1.21	0.04	16.70	0.11	0.01	0.00	2.37
5	51	1.75	0.15	10.19	0.14	0.01	0.00	2.24
5	75	1.65	0.15	13.94	0.19	0.09	0.00	2.33
5	90	0.49	0.08	7.49	0.27	0.08	0.00	2.86
5	110	1.13	0.11	25.65	0.12	0.21	1.54	3.64
5	130	1.81	0.06	39.83	0.04	0.41	4.39	5.23
5	202	2.59	0.39	67.15	0.00	0.82	11.60	11.84
5	401	3.65	0.40	131.07	0.00	1.75	25.17	37.89
5	600	4.05	0.25	238.34	0.01	2.70	37.82	75.91
5	800	6.83	0.63	297.16	0.00	3.16	43.95	107.97
5	941	6.25	0.46	310.76	0.00	3.27	45.07	123.30
6	2	2.85	0.21	6.73	0.08	0.18	0.00	0.01
6	26	1.67	0.73	11.24	0.14	0.10	0.00	1.62
6	36	1.77	0.35	10.20	0.12	0.10	0.00	1.83
6	71	1.33	0.06	8.60	0.22	0.12	0.00	2.09
6	82	2.61	0.10	14.19	0.44	0.26	1.26	2.90
6	100	1.92	0.13	28.09	0.30	0.35	2.90	3.58
6	131	2.14	0.58	47.75	0.12	0.61	7.84	7.40
6	171	1.99	0.37	58.54	0.01	0.88	12.80	12.93
6	211	2.50	0.12	78.38	0.00	1.10	16.43	18.00
6	410	4.52	0.18	161.86	0.00	2.13	31.69	48.01
6	610	4.78	0.13	252.78	0.00	2.88	42.40	85.86
6	810	5.88	0.32	296.37	0.00	3.14	45.93	112.03
6	960	7.20	0.02	310.71	0.00	3.21	46.83	126.98
7	2	1.59	0.33	4.88	0.18	0.09	0.00	1.68
7	31	2.20	0.02	11.17	0.35	0.14	0.00	0.01
7	45	1.54	0.25	19.00	0.85	0.18	0.00	0.37
7	56	2.49	0.12	23.34	0.36	0.28	1.06	1.07
7	85	2.02	0.04	21.57	0.06	0.39	3.45	2.46
7	110	2.67	0.11	33.04	0.02	0.53	6.46	5.23
7	140	2.88	0.04	50.36	0.01	0.78	11.11	10.43
7	170	2.64	0.13	53.28	0.00	0.87	12.85	14.54
7	211	2.86	0.10	72.96	0.00	1.12	20.52	20.88
7	410	4.91	0.50	182.78	0.00	2.11	31.49	52.61
7	602	6.41	0.44	258.69	0.00	2.81	41.09	88.91
7	810	7.33	0.98	299.00	0.00	3.07	44.80	114.79
7	960	4.81	0.20	308.78	0.00	3.14	45.93	128.42

Table S2 (Continued).

8	2	4.49	0.38	10.21	0.24	1.10	11.15	16.55
8	26	4.70	0.20	26.52	0.34	1.11	12.18	18.16
8	63	3.37	0.59	18.74	0.34	1.29	14.72	21.16
8	70	2.85	0.62	21.72	0.18	1.34	15.91	22.67
8	106	3.28	0.60	30.12	0.04	1.64	21.68	30.08
8	140	4.43	0.94	107.36	0.06	1.93	26.94	40.34
8	211	4.52	0.73	209.47	0.01	2.57	37.59	64.27
8	310	4.84	0.53	255.03	0.00	2.88	42.52	81.28
8	410	4.92	0.38	278.85	0.00	3.02	44.16	94.57
8	570	5.86	1.28	292.74	0.00	3.08	44.78	111.05
8	810	5.08	1.02	303.95	0.00	3.16	45.11	130.20
8	960	7.84	1.65	306.84	0.00	3.15	45.70	138.98

Appendix B: Profile Figures for All Stations

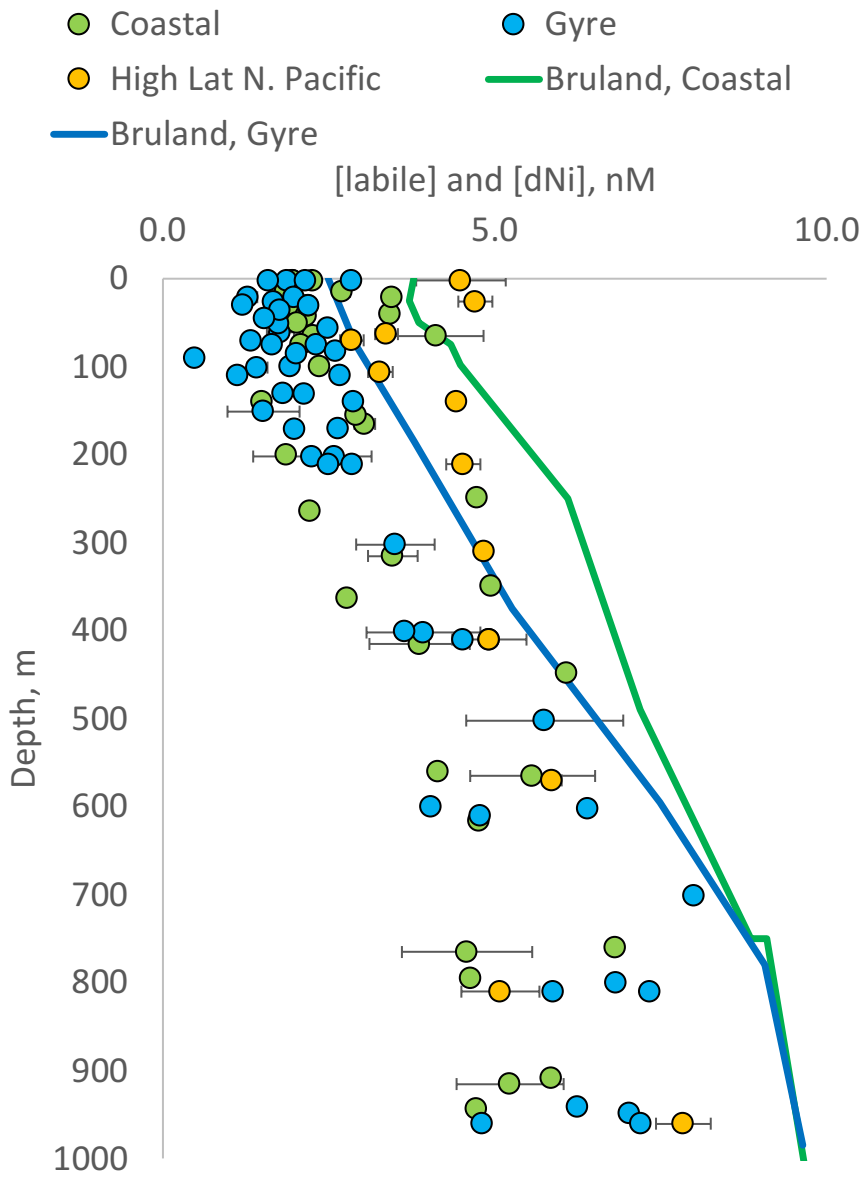

Figure S1. Depth profiles of labile and total dissolved Ni concentrations in the upper 1,000 m of the North Pacific. Filled circles represent labile Ni concentrations from this study separated by ocean regime where green, blue, and yellow represent coastal upwelling, oligotrophic gyre, and Fe limitation, respectively. Total dissolved Ni concentration data shown in lines are from Bruland 1980 with darker green and blue representing coastal and gyre systems, respectively.

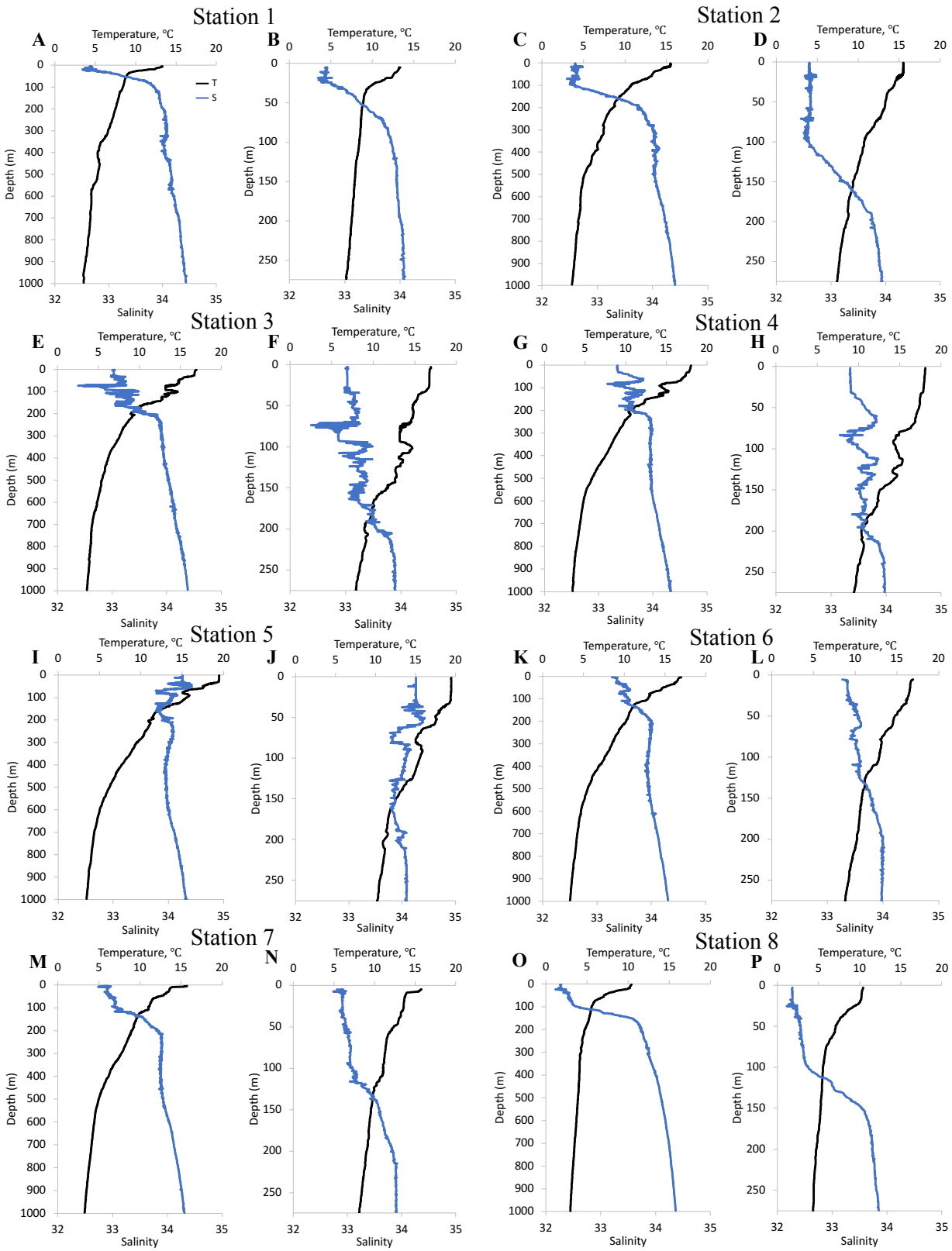

Figure S2. Depth profiles of temperature (top axes, black lines) and salinity (bottom axes, blue lines) from Stations 1 through 8 sampled in the Northeast Pacific. Left panel for each station shows the profile to 1,000 m. Right panel shows profile to 275 m. Figure panels are grouped by station.

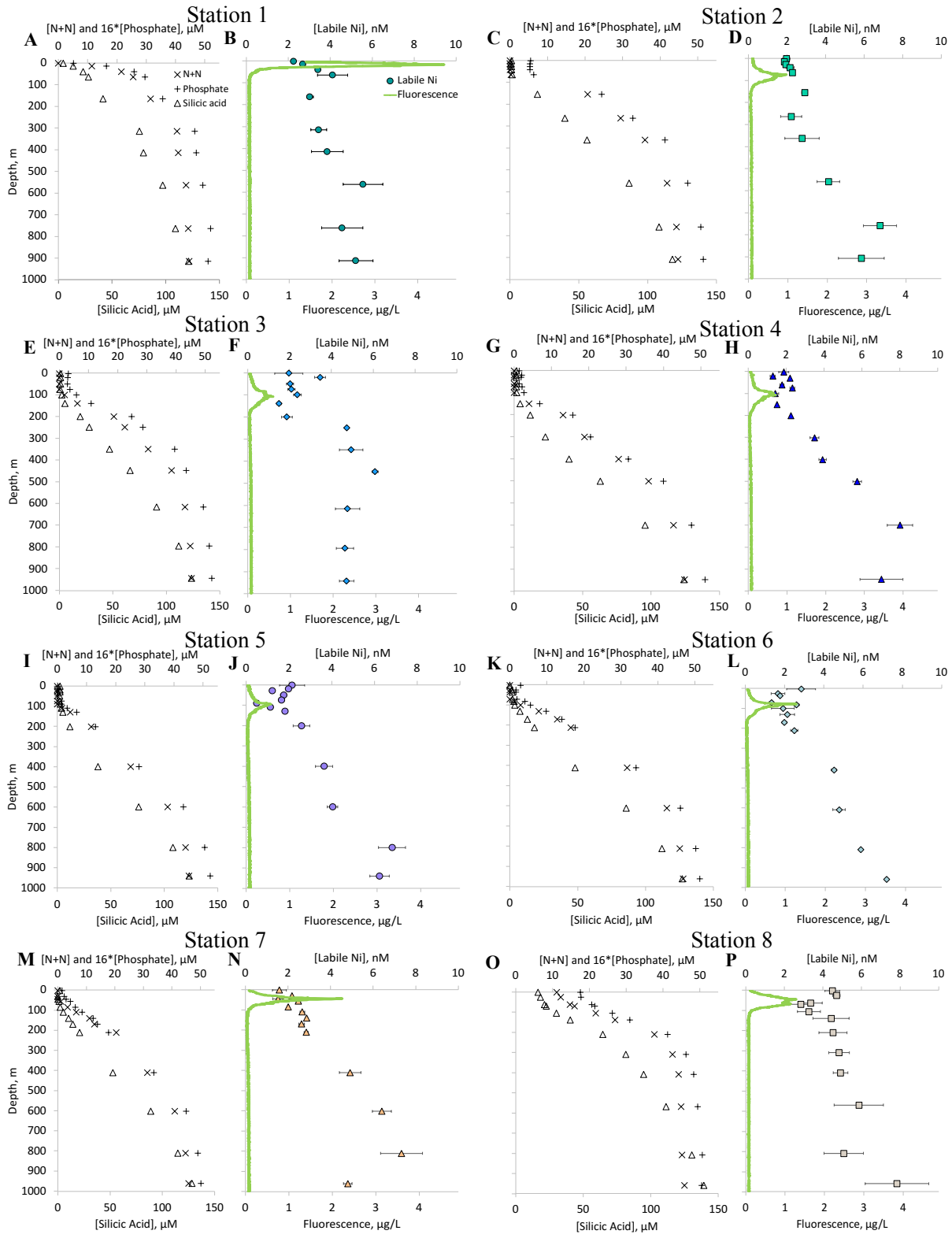

Figure S3. Depth profiles of macronutrients and labile dissolved Ni concentrations in the upper 1,000 m of the Northeast Pacific. Left panels for each station show profiles of nitrate+nitrite (N+N), 16*phosphate (top axes), and of silicic acid (bottom axes) concentrations. Right panels show profiles of labile Ni concentrations (top axes) and of fluorescence (bottom axes). Figure panels are grouped by station.

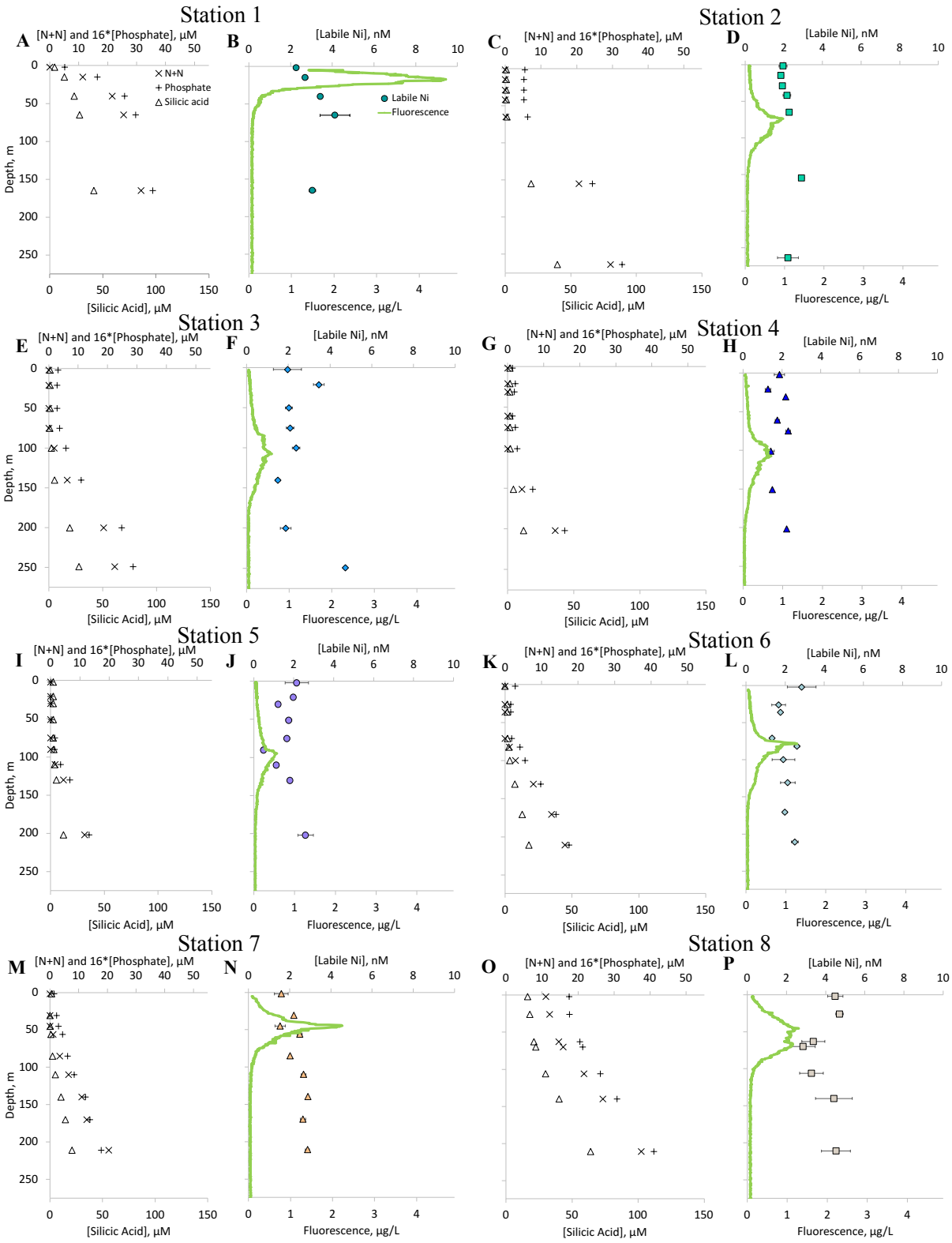

Figure S4. Depth profiles of macronutrients and labile dissolved Ni concentrations in the upper 275 m of the Northeast Pacific. Left panels for each station show profiles of nitrate+nitrite (N+N), 16*phosphate (top axes), and of silicic acid (bottom axes) concentrations. Right panels show profiles of labile Ni concentrations (top axes) and of fluorescence (bottom axes). Figure panels are grouped by station.

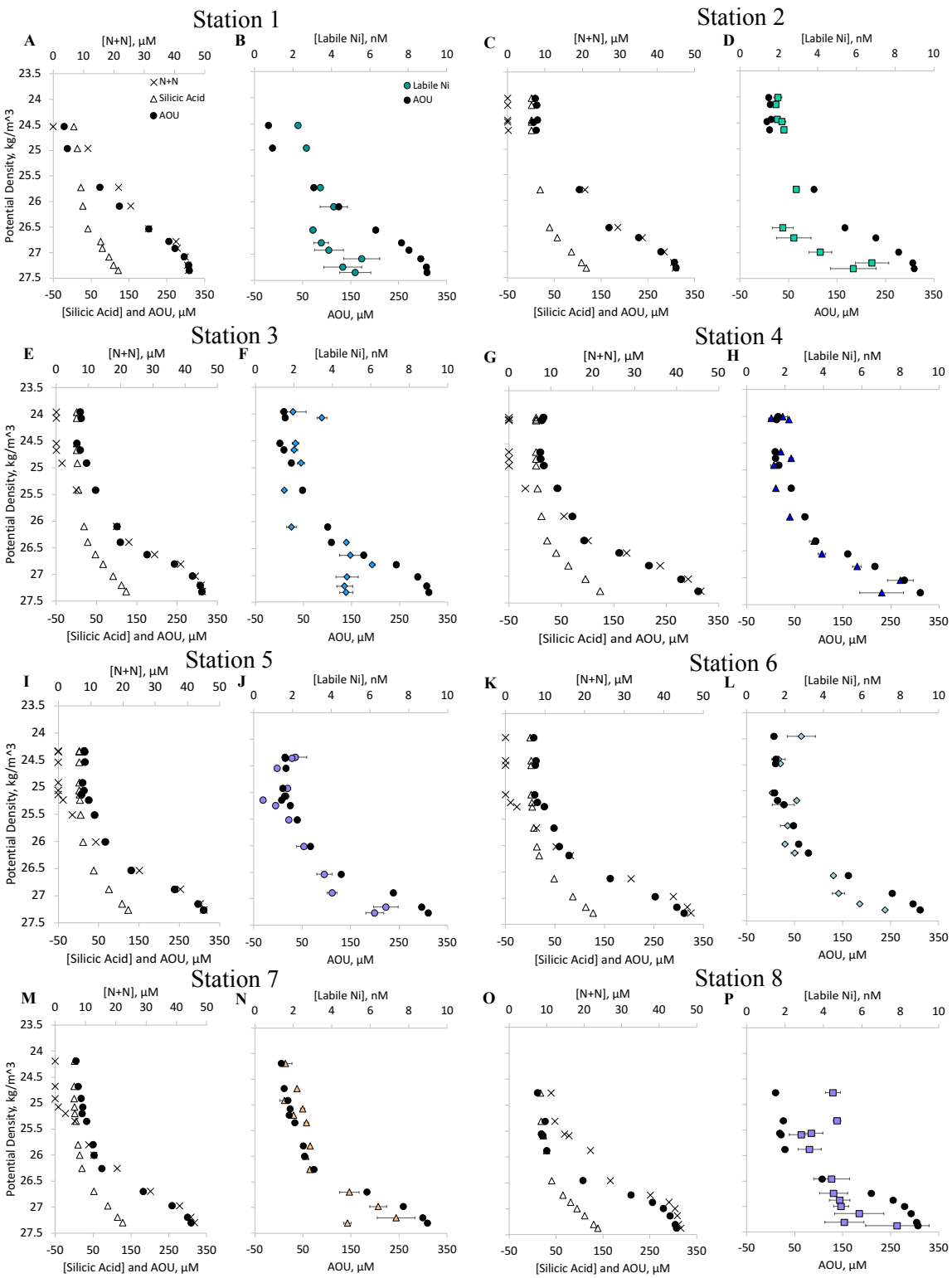

Figure S5. Profiles of AOU and macronutrient concentrations in the Northeast Pacific as a function of potential density. Left panels for each station show profiles of AOU (bottom axes), with nitrate+nitrite (N+N, upper axes), and silicic acid (bottom axes) concentrations. Right panels show profiles of AOU (bottom axes) with labile dissolved Ni concentrations (top axes). Figure panels are grouped by station.